INCREASE OF FRACTURE RESISTANCE BY THE INTERACTION OF TWO CRACKS COHESIVE LAW SCALE EFFECTS

BENT F. SØRENSEN AND STERGIOS GOUTIANOS

Section of Composites and Materials Mechanics,
Department of Wind Energy, Technical University of Denmark,
DK-4000 Roskilde, Denmark.
E-mail: bsqr@dtu.dk, gout@dtu.dk
URL: http://www.vindenergi.dtu.dk

Key words: Multiple Cracks, Fracture Resistance, Delamination, Cohesive Law

Abstract. The increase of the fracture resistance of a layered structure by adding weak layers is examined through a finite element model containing two cracks. The cracks are modelled as cohesive zones. The cohesive law parameters, such as the critical opening relative to the specimen size, introduce scale effects. It is shown that a maximum increase of the fracture resistance can be attained for certain cohesive law parameters even when the distance between the two cracks is relative large relative to the structure dimensions.

1 INTRODUCTION

Through-thickness stresses can cause initiation and propagation of interlaminar cracks which may lead to a decrease of the structural integrity of a composite component [1]. An example is cracks initiated at ply-drops in wind turbine blades. A number of techniques have been developed to increase the fracture resistance of composites by making the damage prone areas stronger or tougher. This is achieved by using tougher matrices [2, 3], modifying the fibre/matrix interface [4, 5], using interleaving concepts [6, 7] or by modifying the fibre architecture e.g. z-pinning [8].

An alternative approach to increase the fracture resistance was proposed by Goutianos and Sørensen [9]. The fracture resistance is increased by introducing weak planes next to the damage prone areas and thus allowing the initiation and propagation of multiple cracks as shown in Fig. 1 for the case of two cracks. This approach was motivated by the experimental work of Rask and Sørensen [10] who observed, in testing Double Cantilever Beam (DCB) specimens, that a change of the ply thicknesses of the glass fibre/polyester composite beams bonded together with an adhesive, more delamination cracks could develop next to the adhesive/laminate crack. In these experiments, the steady-state fracture resistance was found to increase proportionally to the number of secondary (delamination) cracks, suggesting that a linear relationship may exist between the number of crack tips/fracture process zones and the steady state fracture resistance.
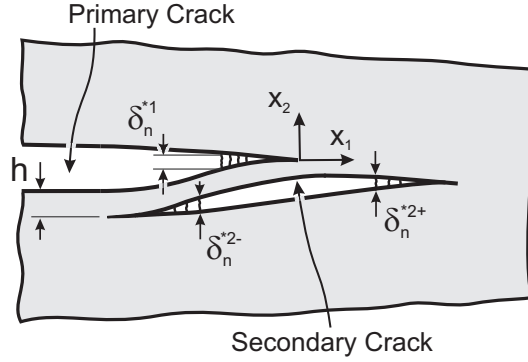
Figure 1: Delamination of a weak layer (secondary crack)at a distance h from the primary crack. $\delta_n^{*,1}$ is the normal end-opening of the primary crack, $\delta_n^{*,2-}$ and $\delta_n^{*,2+}$ the normal end-openings of the right and left hand side crack tips of the secondary crack. The corresponding tangential end-openings of the primary and secondary cracks are $\delta_t^{*,1}$, $\delta_t^{*,2-}$ and $\delta_t^{*,2+}$.

In the present work, the possibility of increasing the fracture resistance of a layered structure by introducing weak planes (resulting in multiple delaminations) next to a damage prone area is further investigated by exploring the effects of the cohesive law parameters. It should be noted that in many layered structures such as fibre composite materials [5] or adhesive joints [11], crack growth/delamination involves large scale fibre bridging and thus the problem cannot be analysed by linear elastic fracture mechanics.

2 BACKGROUND

The mechanism of multiple delaminations formation of Fig. 1 was analysed in Goutianos and Sørensen [9] for two cracks/delaminations. Using the path independent J integral [12], it was shown that the J integral along a local path enclosing the primary and secondary crack, see Fig. 2, is:

$$J_{loc} = J_{loc}^1 + J_{loc}^{2-} + J_{loc}^{2+} \tag{1}$$

where if the primary crack is fully developed then $J_{loc}^1 = J_{ss}^1$. If the right hand side secondary crack is fully developed then, $J_{loc}^{2+} = J_{ss}^2$. Similarly, if the left hand side secondary crack is fully developed, $J_{loc}^{2-} = J_{ss}^2$. If it is assumed, that the left hand side of the crack tip of the secondary crack does not open, then $J_{loc}^{2-} = 0$, and thus:

$$J_{loc} = J_{loc}^1 + J_{loc}^{2+} = J_{ss}^1 + J_{ss}^2 \tag{2}$$

which shows that the steady fracture resistance, $J_{R,ss}$, is increased by J_{ss}^2. Eq. 2 can be generalised to n secondary/delaminations cracks:

$$J_{loc} = J_{ss}^1 + n J_{ss}^2 \tag{3}$$

If left hand side of the secondary crack is fully developed, then Eq. 1 gives that $J_{loc} = J_{ss}^1$ *e.g.* there is no increase in the steady state fracture resistance.
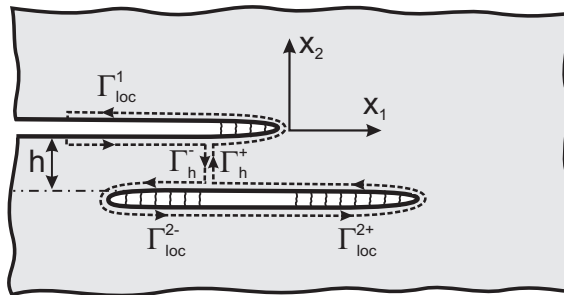
Figure 2: Local J integral path enclosing the primary and secondary crack.

3 NUMERICAL MODEL

3.1 Geometry and loading

The crack growth problem of Fig. 1 is modelled by the finite element method using the commercial code Abaqus (version 2017) as a plane strain problem (see Fig. 3). The right hand side is fully constrained ($u_1 = u_2 = 0$ at $x_1 = L - \ell$). Pure bending is applied to the left hand side beams by prescribing rotational displacements of two points, which are tied to two analytical rigid surfaces tied to the beams of the specimen. The two beams are modelled as plane strain isotropic linear-elastic solids. Four-node elements and triangular three-node reduced integrations elements are used in order to control the mesh transition from the small size elements in the cohesive zone to larger elements far away from the cohesive zones.

An explicit solver is used to solve the problem under quasi-static conditions using mass-scaling [11]. In the solution procedure, viscous damping is also necessary for convergence. In all simulations, it is ensured that the sum of the kinetic energy and the energy dissipated by viscosity is less than 0.5% of the strain energy.

The J integral evaluated along the external boundaries, under plane strain conditions and mixed-mode loading, is [13]:

$$J_{ext} = (1 - \nu^2)\frac{21(M_1^2 + M_2^2) - 6M_1M_2}{4B^2H^3E} \tag{4}$$

where H and B are the height and width of the specimen, E and ν are the Youngs' modulus and Poisson's ratio of the beams and the moments M_1 and M_2 applied to the left hand cracked ends of the beams. The moments M_1 and M_2 are extracted from the finite element solution for each increment. Eq. 4 is valid only as long as the secondary crack remains away from the left hand end of the beam so that the beams ends are subjected to pure bending. As can be seen from Eq. 4 the J integral equation is independent of the crack length. Thus, by extracting the moments from the finite element solution, the fracture resistance, J_R, given by the J integral can be directly evaluated.

3.2 Cohesive zone modelling

The potential planes for the primary and secondary cracks are modelled with cohesive elements of finite thickness corresponding to 0.1% of H (see Fig. 3) to avoid interpene-
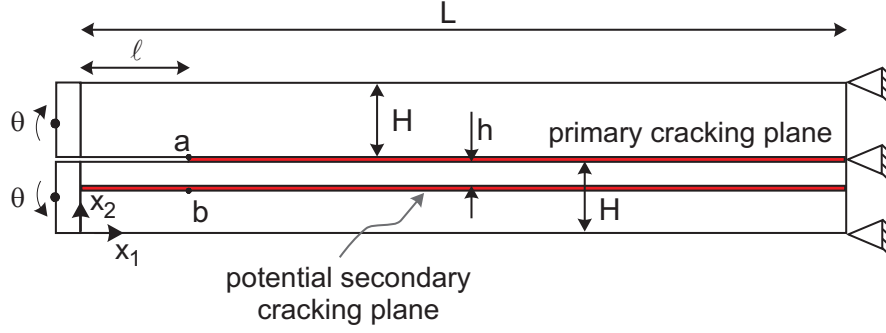
Figure 3: Geometry, loads and boundary conditions of the finite element model. The potential cracking planes (for the primary and secondary cracks) are modelled with cohesive zones.
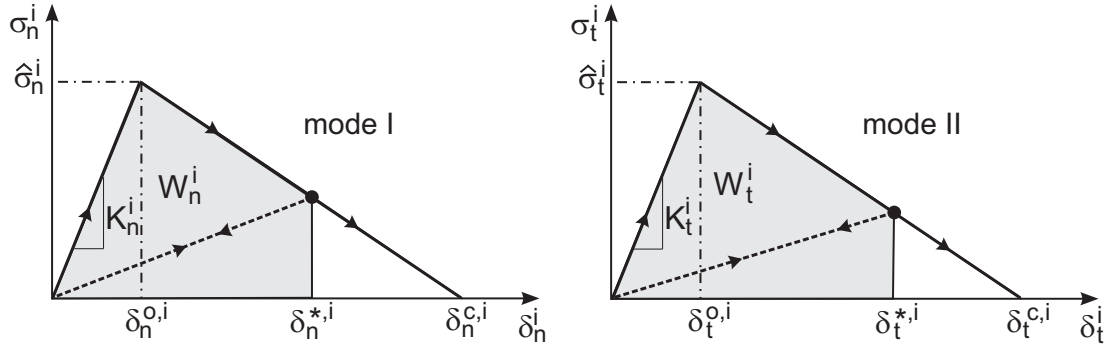

Figure 4: Mode I and mode II linear softening cohesive laws for the primary ($i=1$) and secondary crack ($i=2$).

tration of the two surfaces adjacent to the cohesive elements. The cohesive zone of the potential secondary crack plane extends along the entire length the specimen, L, allowing thus crack growth behind the initial notch (primary crack).

The cohesive laws have a bilinear shape as can be seen in Fig. 4, which shows the pure normal and shear cohesive laws for each crack where σ_n^i and σ_t^i are the normal and shear tractions ($i = 1$: primary crack and $i = 2$: secondary crack), δ_n and δ_t the normal and tangential openings. The cohesive laws have initial rising parts with stiffness K_n^i and K_t^i for the primary and secondary cracks which are assigned high values ($K_n^i H/E = K_t^i H/E = 2.5 \times 10^{-3}$) to practically have linear softening cohesive laws with minimum opening prior to crack opening.

Although the external applied loading corresponds to pure mode I crack opening, the presence of the secondary crack introduces tangential openings to both the primary and secondary crack. Following the mixed-mode cohesive zone model of [14], it is assumed that the normal and shear cohesive laws are uncoupled. A weak coupling is introduced through a failure criterion:

$$F_{cr} = \frac{W_n^i}{J_{n,ss}^i} + \frac{W_t^i}{J_{t,ss}^i} = 1, \quad i = 1 \quad or \quad 2 \tag{5}$$

where $J_{n,ss}^i$ and $J_{t,ss}^i$ are the mode I and mode II steady state fracture resistances for the

primary ($i = 1$) and for the secondary crack ($i = 2$). The work of the cohesive tractions (shaded area in Fig. 4) are denoted W_n and W_t for the normal and shear tractions, respectively. With the uncoupled cohesive law chosen, W_n and W_t depend only on δ_n^* and δ_t^*, respectively.

The cohesive law is implemented in a user defined material subroutine. Since, a basic assumption of the analytical model [9] is that the left hand side of the secondary crack can unload, the unloading behaviour is also implemented and is is shown with dotted lines in Fig. 4.

4   RESULTS AND DISCUSSION

Fig. 5 shows the steady state fracture resistance for a specimen with two cracks as a function of the distance between the two cracks, h, for different ratios of the normal peak traction of the secondary crack to the normal peak traction of the primary crack, $\hat{\sigma}_n^2/\hat{\sigma}_n^1$. For both cracks a) the pure mode II cohesive law is identical to the pure mode I cohesive law and b) $J_{n,ss}^1$ and $J_{n,ss}^2$. For all cases plotted in Fig. 5, $J_{n,ss}^1/(EH) = 2.5E^{-6}$. When the secondary crack is at a small distance from the primary crack ($h/H < 0.4$), then the steady state fracture resistance is close to the analytical solution of Eq. 2, $e.g.$ the steady state fracture resistance is the sum of the steady state fracture resistances of the two cracks. This maximum positive contribution from the secondary crack occurs when the peak traction is of the secondary crack is close but smaller to the peak traction of the primary crack. When the peak traction of the secondary crack is less than half the peak traction of the primary crack, then the analytical solution of Eq. 2 is achieved only for small distances h $e.g.$ $h/H < 0.2$. In all cases, when the two cracks are relatively apart from each other ($h/H < 0.6$), then the fracture resistance does not reach its upper theoretical limit (Eq. 2) due to the negative contribution from the left hand side crack tip of the secondary crack [9]. When, the peak traction of the secondary crack is larger than the peak traction of the primary crack, then the secondary crack does not open and the steady state fracture resistance is equal to the steady state fracture resistance of the primary crack.

The results of Fig. 5 show that it is feasible to increase the fracture resistance of a layered structure significantly by adding weak layers as long as the cohesive law parameters of the weak layers are within certain ranges compared to the cohesive law parameters of the primary crack. However, the maximum positive effect of the secondary crack occurs only when the secondary crack is at a short distance from the primary crack. In many practical cases, such as in composite structures, it may be difficult to introduce a weak layer at a small distance h due to geometrical constraints such as lamina thickness. Thus, it is important to examine if it is possible to increase the fracture resistance even when the weak layer is relatively far apart from the primary crack.

Next in Fig. 6, the cohesive law parameters of the primary crack are also varied. More specifically, the mode I peak traction is increased whereas the mode I steady state fracture resistance is kept constant compared to the cohesive law parameters of the primary crack in Fig. 5, $J_{n,ss}^1/(EH) = 2.5E^{-6}$. By increasing the mode I peak traction and keeping the steady state fracture resistance constant, the mode I critical opening decreases $e.g.$ the
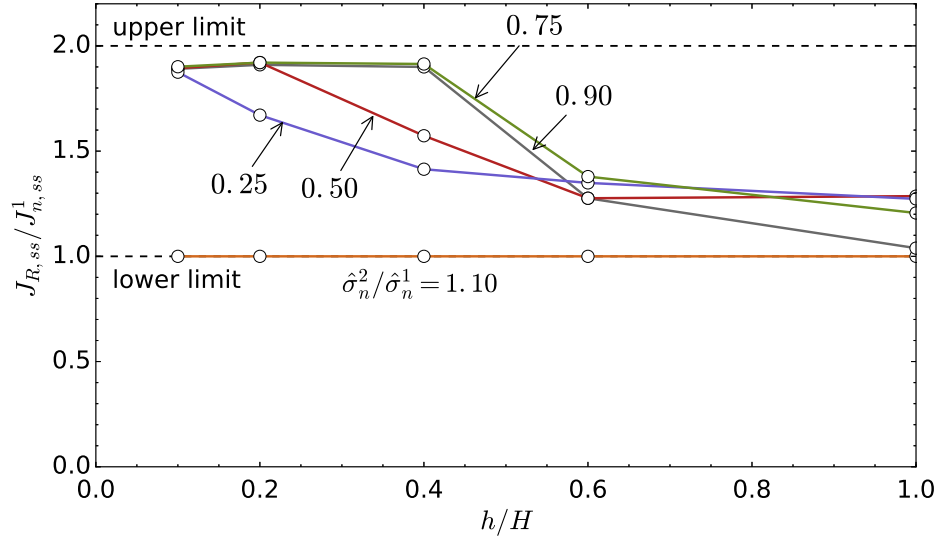
5

Figure 5: Steady state fracture resistance, $J_{R,ss}$, as a function of a distance between the two cracks h for different peak traction ratios of $\hat{\sigma}_n^2/\hat{\sigma}_n^1$. The mode II cohesive law is identical to the mode I cohesive law for each crack. $\hat{\sigma}_n^1/E = 5.0E - 5$.

critical opening is decreases relatively to H. In Fig. 6, the steady state fracture resistance is shown as a function of the ratio of the mode II peak traction of the secondary crack to the mode I peak traction of the primary crack when the two cracks are far apart from each other ($h/H = 0.1$). For this distance, the increase of the steady state fracture resistance was only up to 20% when $\hat{\sigma}_n^1/E = 5.0E - 5$ (see Fig. 5). It should be mentioned that in the results of Fig. 6, the mode II cohesive law of the primary crack is identical to the mode I cohesive law of the primary crack. Similarly, the mode II cohesive law of the secondary crack is identical to the mode I cohesive law of the secondary crack. It can be seen that increasing the mode I peak traction of the primary crack results in a significant increase of the fracture resistance for a wide range of ratios of the mode I peak traction of the secondary crack to the mode I peak traction of the primary crack. When $\hat{\sigma}_n^1/E = 5.0E - 4$, then the steady state fracture resistance reaches the upper theoretical limit given in Eq. 2.

The implication of the results of Fig. 6 is that it is feasible to increase the fracture resistance when the weak layer is relatively far apart from the primary crack, only if the cohesive law parameters of the primary crack are within certain ranges compared to the specimen dimensions. This implies that it may be necessary first to modify the cohesive law parameters of the primary crack (damage prone area) and secondly design/modify the cohesive law parameters of the weak layer relatively to the primary crack.
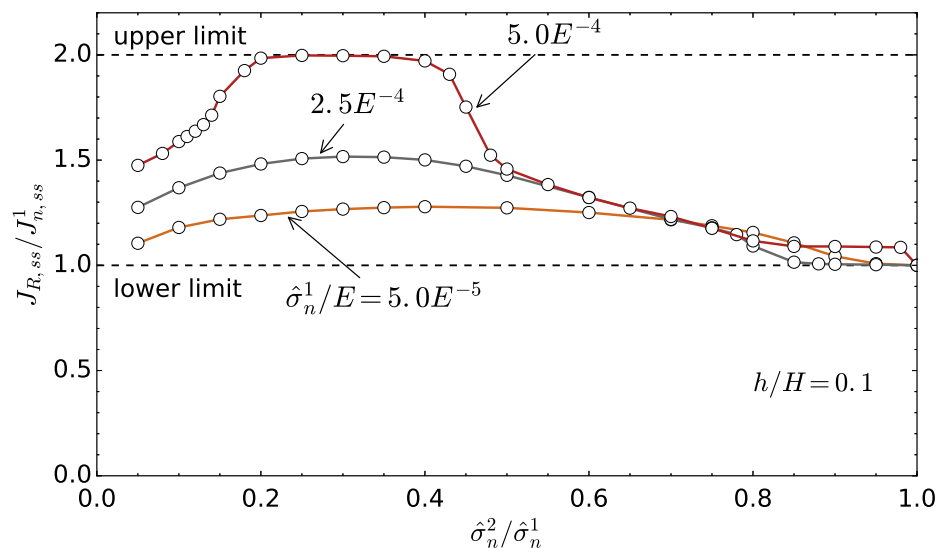
Figure 6: Steady state fracture resistance, $J_{R,ss}$, as a function of a .

5   CONCLUSIONS

Cohesive zone modelling, consisting of a primary and a secondary crack, was used to demonstrate that it is possible to significantly increase the fracture resistance of a layered structure by adding weak layers. It was shown that by selecting the cohesive law parameters of the secondary crack within certain ranges, a linear dependency between the number of cracks and the steady state fracture resistance can be achieved in accordance to theoretical predictions. This linear dependency also holds when the two cracks are far apart for certain ranges of the cohesive law parameters of both the primary and secondary crack.

6   ACKNOWLEDGMENTS

REFERENCES

[1] Dransfield, K.A., Jain, L.K. and Mai, Y.W. On the effects of stitching in CFRPs – I. Mode I delamination toughness. *Compos. Sci. Technol.* (1998) **58**:815–827.

[2] Kim, J.K., Ballie, C., Poh, J. and Mai, Y.W. Fracture toughness of CFRP with modified epoxy matrices. *Compos. Sci. Technol.* (1992) **43**:283–297.

[3] Kinloch, A., Masania, K., Taylor, A., Sprenger, S. and Egan, D. The fracture of glass-fibre reinforced epoxy composites using nanoparticle-modified matrices. *J. Mater. Sci.* (2008) **43**:1151–1154.

[4] Madhukar, M. and Drzal, L.T. Fibre-matrix adhesion and its relationship to composite mechanical properties. *J. Mater. Sci.* (1993) **28**:569–610.

[5] Feih, S., Wei, J., Kingshott, P. and Sørensen, B.F. The influence of fibre sizing on the strength and fracture toughness of glass fibre composites. *Composites Part A* (2005) **36**:245–255.

[6] Hojo, M., Matsuda, S., Tanaka, M., Ochiai, S. and Murakami, A. Mode I delamination fatigue properties of interlayer-toughened CF/epoxy laminates. *Compos. Sci. Technol.* (2006) **66**:665–675.

[7] Wong, D.W.Y., Lin, L., McGrail, P.T., Peijs, T., Hogg, P.J. Improved fracture toughness of carbon fibre/epoxy composite laminates using dissolvable thermoplastic fibres. *Composites Part A* (2010) **41**:759–767.

[8] Mouritz, A.P. Review of z-pinned composite laminates. *Compos. Part A Appl. Sci.* (2007) **38**:2383–2397.

[9] Goutianos, S. and Sørensen, B.F. Fracture resistance enhancement of layered structures by multiple cracks. *Engng. Fract. Mech.* (2016) **151**:92–108.

[10] Rask, M. and Sørensen, B.F. Determination of the J integral for laminated double cantilever beam specimens: the curvature approach. *Engng. Fract. Mech.* (2012) **96**:37–48.

[11] Sørensen, B.F., Goutianos, S., Jacobsen, T.K. Strength scaling of adhesive joints in polymer-matrix composites. *Int. J. Solids Struct.* (2009) **46**:741–761.

[12] Rice, J.R. A path independent integral and the approximate analysis of strain concentrations by notches and cracks. *J. Appl. Mech.* (168) **35**:379–386.

[13] Sørensen, B.F., Jørgensen, K., Jacobsen, T.K. and Østergaard, R.C. DCB-specimen loaded with uneven bending moments. *Int. J. Fract.* (2006) **141**:163–176.

[14] Yang, Q.D., and Thouless, M.D. Mixed-mode fracture analyses of plastically-deforming adhesive joints. *Int. J. Fract.* (2001) **110**:175–187.